HHS Public Access

Author manuscript

Cell Rep. Author manuscript; available in PMC 2019 August 11.

Published in final edited form as:

Cell Rep. 2019 January 02; 26(1): 37–44.e7. doi:10.1016/j.celrep.2018.12.035.

A chaperone lid ensures efficient and privileged client transfer during tail-anchored protein targeting

Un Seng Chio[1], **SangYoon Chung**[2], **Shimon Weiss**[2], **Shu-ou Shan**[1,3,*]

[1]Division of Chemistry and Chemical Engineering, California Institute of Technology, Pasadena, CA 91125

[2]Department of Chemistry and Biochemistry, University of California Los Angeles, Los Angeles, CA 90095

[3]Lead Contact

Summary

Molecular chaperones play key roles in maintaining cellular proteostasis. In addition to preventing client aggregation, chaperones often relay substrates within a network while preventing off-pathway chaperones from accessing the substrate. Here we show that a conserved lid motif lining the substrate-binding groove of the Get3 ATPase enables these important functions during the targeted delivery of tail-anchored membrane proteins (TAs) to the endoplasmic reticulum. The lid prevents promiscuous TA handoff to off-pathway chaperones, and more importantly, it cooperates with the Get4/5 scaffolding complex to enable rapid and privileged TA transfer from the upstream co-chaperone Sgt2 to Get3. These findings provide a molecular mechanism by which chaperones maintain the pathway specificity of client proteins in the crowded cytosolic environment.

Keywords

chaperone; protein targeting; tail-anchored protein; ATPase; membrane protein

Introduction

Protein homeostasis requires the proper folding, assembly, and localization of proteins inside a cell. Molecular chaperones play key roles in maintaining protein homeostasis by protecting their client proteins from off-pathway interactions and guiding the folding or localization of client proteins (Kim et al., 2013). Newly synthesized membrane proteins, which comprise up to 30% of the proteins encoded in the genome, are particularly challenging clients for chaperones due to the high aggregation propensity of hydrophobic transmembrane domains (TMDs) in the cytosol, where membrane proteins are initially synthesized. In addition,

*corresponding author. sshan@caltech.edu.

Author contributions

U.S.C. and S.-o.S. designed the research; U.S.C. performed biochemical experiments; U.S.C. analyzed biochemical data with input from S.-o.S.; U.S.C. and S.C. performed single-molecule fluorescence experiments; U.S.C. and S.C. analyzed the data with input from S.W. and S.-o.S.; U.S.C and S.-o.S. wrote the manuscript; all authors approved the final manuscript.

Declaration of interests

The authors declare no competing interests.

TMDs are often degenerate in sequence, amino acid composition, and secondary structure propensity, making them susceptible to promiscuous interactions with off-pathway chaperones. Therefore, chaperones that engage integral membrane proteins not only need to effectively capture and shield client proteins from solvent, but also ensure that substrates remain on-pathway en route to the target membrane. Although recent advances defined the substrate binding domains and client interactions for a variety of membrane protein chaperones (Burmann et al., 2013; Huang et al., 2016; Liang et al., 2016; Thoma et al., 2015), how these chaperones ensure the pathway specificity of substrates remains poorly understood.

Here we address this question in the conserved Guided Entry of Tail-anchored protein (GET) pathway, which mediates the targeted delivery of tail-anchored membrane proteins (TAs) to the endoplasmic reticulum (ER) in eukaryotic cells (Figure S1A) (Chio et al., 2017a; Hegde and Keenan, 2011). At the center of this pathway is the ATPase Get3 (or mammalian TRC40) (Stefanovic and Hegde, 2007), which captures TAs from the upstream co-chaperone Sgt2 (or mammalian SGTA) (Wang et al., 2010). The Sgt2-to-Get3 TA transfer is facilitated by ATP and the scaffolding complex Get4/5, which together pre-organize Get3 into a *closed* and ATPase-inhibited conformation optimal for TA capture (Gristick et al., 2014, 2015; Rome et al., 2013). TA loading induces rapid opening motions in Get3 and activates ATP hydrolysis (Chio et al., 2017b; Rome et al., 2013), which drives Get3 to switch its interaction partner from Get4/5 to the Get1/2 receptors at the ER membrane (Chio et al., 2017b; Schuldiner et al., 2005, 2008).

The TA-TMD docks into a hydrophobic groove formed by ATP- and Get4/5-bound Get3 (Mateja et al., 2009, 2015). Moreover, the transfer of TA from SGTA to TRC40 was not perturbed by excess calmodulin (CaM), an external chaperone (Shao and Hegde, 2011) that also binds TAs, indicating that TAs are protected from off-pathway chaperones during their transfer (Shao et al., 2017). Nevertheless, as hydrophobic interactions are short-ranged, it is unclear how TAs are loaded into the deep TMD-binding groove of Get3, nor how they are shielded from solvent and external chaperones during and after loading. Intriguingly, a conserved helix 8 (α8; Figures S1B and S1C) lines the substrate-binding groove of Get3 (Mateja et al., 2009, 2015). Although α8 is unresolved in most Get3 structures (Figure S1C) (Gristick et al., 2014, 2015; Hu et al., 2009; Mateja et al., 2009, 2015), it can be crosslinked to TAs (Mateja et al., 2015). Mutation of conserved α8 residues resulted in yeast growth defects under stress conditions (Mateja et al., 2009) and impaired Get3-dependent TA targeting in yeast lysate (Rome et al., 2013). It was hypothesized that α8 acts as a dynamic lid to enclose the TA binding groove and prevent TAs from aggregation (Mateja et al., 2015). In other chaperones or targeting factors, such as Hsp70 (Mayer and Bukau, 2005) and the signal recognition particle (Akopian et al., 2013), a lid motif lining the substrate binding groove could also stabilize substrate binding or mediate substrate-induced conformational changes.

Here, quantitative biochemical and biophysical analyses revealed unexpected roles of α8 in Get3 function. We found that, although α8 is not necessary for maintaining a stable Get3•TA complex, it nevertheless prevents TA loss from Get3 to off-pathway chaperones. Most importantly, α8 acts synergistically with Get4/5 to enable rapid TA transfer from Sgt2 to

Get3 in a highly protected manner. We propose that α8 forms a molecular conduit for TA transfer to Get3, illustrating a mechanism that chaperones use to ensure client-pathway specificity in a crowded cytosolic environment.

Results

α8 is necessary for efficient TA targeting

Previously, it was shown that mutation of conserved α8 residues (M200D and L201D) resulted in yeast growth defects under stress conditions, which is characteristic of defects in the GET pathway (Mateja et al., 2009). Different mutations of α8 also impaired Get3-dependent TA targeting to different extents in yeast lysate (Rome et al., 2013). To unambiguously assess the role of α8, we engineered a Get3 mutant in which the highly conserved hydrophobic residues in α8 were replaced by a glycine-serine linker (Figure S1B, Get3(Δα8)) (Chio et al., 2017b). Four lines of evidence show that the Δα8 mutation did not cause nonspecific structural defects in Get3. First, purified Get3(Δα8) migrated as a well-defined, homogeneous peak on size-exclusion chromatography similarly to wild-type Get3 (Figures S2A and S2B). Second, Get3(Δα8) adopted the same global fold as wild-type Get3 as determined by circular dichroism (Figure S2C). Third, Get3(Δα8) hydrolyzed ATP at rates similar to those of wild-type Get3 (Figure S2D). Fourth, Get3(Δα8) displayed ATP-dependent high affinity binding to Get4/5 similar to wild-type Get3 (Figures S2E and S2F). Finally, Get3(Δα8) displayed a similar conformational distribution and underwent conformational regulations by nucleotides, Get1, and Get4/5 similarly to wild-type Get3 (Figure S3), as determined by a previously established single-molecule FRET assay for monitoring global Get3 conformations (Chio et al., 2017b).

We first measured the ability of purified Get3(Δα8) to target and translocate *in vitro* translated TAs into yeast rough microsomes (yRMs) in a *Δget3* yeast lysate (Rome et al., 2013; Wang et al., 2010), assessed by glycosylation of an engineered opsin tag on the model TA upon successful insertion into the ER. Get3(Δα8) exhibited a strong defect in this reconstituted targeting reaction (Figure S1D), indicating that α8 is necessary for Get3 function. To test if Get3(Δα8) compromised TA targeting *in vivo*, we replaced genomic *GET3* in *S. cerevisiae* with *GET3-FLAG* or *GET3(Δα8)-FLAG* and measured Get3 function *in vivo* using two independent assays. First, we measured the secretion of Kar2p, which is retained in the ER by retrograde trafficking in wild-type cells but is secreted into media from *Δget3* cells due to defective biogenesis of SNARE proteins (a large class of TAs) (Schuldiner et al., 2005, 2008). *GET3(Δα8)-FLAG* yeast displayed increased levels of Kar2p secretion compared to *Get3-FLAG* yeast, consistent with compromised GET pathway function (Figure S1E). Second, pulse-chase experiments showed that the insertion of a newly-synthesized model TA, BirA-Bos1-opsin (Cho and Shan, 2018), into the ER was significantly impaired in *GET3(Δα8)-FLAG* compared to *GET3-FLAG* cells (Figure S1F). The defects of *GET3(Δα8)-FLAG* cells cannot be explained by a lower expression level of Get3(Δα8)-FLAG than Get3-FLAG (Figure S1G). These results indicate that the α8 element is also necessary for GET-dependent targeting *in vivo*.

α8 shields TAs from off-pathway chaperones

To test whether α8 helps maintain a stable Get3•TA complex, we measured the kinetic stability of the Get3(Δα8)•TA complex using a FRET assay based on a donor dye incorporated near the TA-TMD and an acceptor dye labeled on Get3 near the substrate binding groove (Rao et al., 2016). We chased a preformed, purified Get3•TA complex with unrelated chaperones that can also effectively bind TAs and monitored TA release from Get3 as a loss of FRET (Figure 1A) (Chio et al., 2017b). We used two independent chase molecules: a superactive variant of cpSRP43, a membrane protein chaperone in the chloroplast of green plants (Jaru-Ampornpan et al., 2010; Schuenemann et al., 1998) and was shown to bind TAs (Cho and Shan, 2018) (Figures 1B and S4A–B); and CaM, another TA-binding protein unrelated to the GET pathway (Shao and Hegde, 2011; Shao et al., 2017) (Figure 1D). When the observed dissociation kinetics were extrapolated to zero chase concentrations to obtain the intrinsic Get3•TA dissociation rate constants ($k_{dissociation}$; Figures 1C and 1E), wild-type Get3•TA and mutant Get3(Δα8)•TA exhibited $k_{dissociation}$ values that are within 2-fold of one another (Figure 1F). Thus, α8 is not required to maintain a kinetically stable Get3•TA complex.

During these measurements, we noticed that the observed kinetics of TA loss from Get3(Δα8) was strongly accelerated by increasing chase concentration (Figures 1B–1E), regardless of whether cpSRP43 or CaM was used as the chase. This kinetic behavior cannot be explained by a model in which the chase molecules acted as an inert TA-trap that simply binds dissociated TAs and prevents their rebinding to Get3(Δα8), as the observed reaction kinetics would be rate-limited by TA dissociation and independent of chase concentration in this model (Figures 1G and S4). Rather, this observation indicates that external chaperones actively stimulate TA release from Get3(Δα8) (Figure 1H, top pathway). In contrast to Get3(Δα8), the observed TA release kinetics of wild-type Get3 was independent of chase concentration (Figure 1C) (Chio et al., 2017b), indicating that the external chaperones act solely as passive TA-traps for wild-type Get3. Thus, although α8 is unnecessary for maintaining a stable Get3•TA complex, it helps Get3 to protect its bound substrate from access by and loss to other chaperones.

α8 and Get4/5 synergistically enable rapid and privileged TA transfer from Sgt2 to Get3

The results above and from previous work (Chio et al., 2017b) showed that the Get3(Δα8)•TA complex displays high kinetic stability. Moreover, purified Get3(Δα8)•TA was insertion-competent (Chio et al., 2017b). We further showed that Get3(Δα8)•TA can mediate TA targeting and insertion into yRMs with the same efficiency as wild-type Get3 even with Get4/5 present (Figure 2A), indicating that the Δα8 mutation does not disrupt TA-induced conformational changes that allows Get3 to exchange its binding partner from Get4/5 to the Get1/2 receptors (Figure S1A, steps 3–4) (Chio et al., 2017b). These observations contrast with the strong defect of Get3(Δα8) in mediating TA targeting in yeast lysate and *in vivo* (Figure S1). Although Get3(Δα8) has a higher tendency to hand off the TA to external chaperones than wild-type Get3, the rate of TA loss from Get3(Δα8) ($k \geq 0.015\ min^{-1}$) is slow compared to that of TA insertion ($k = 0.14\ min^{-1}$; Figure 2A) and unlikely to account for the observed targeting defect of this mutant. As the experiments in yeast lysate and *in vivo* include all the molecular steps in the GET pathway, we

hypothesized that Get3(Δα8) has additional defects in steps prior to the formation of the Get3•TA complex.

The only major upstream step involving Get3 is the transfer of TA from Sgt2 to Get3. To test if α8 is important for this transfer event, we used an established FRET-based assay (Rao et al., 2016) in which acceptor-labeled Get3 is presented to a preformed Sgt2•TA complex in which the TA is labeled with a donor dye (Figure 2B). Successful TA transfer and loading onto Get3 give rise to efficient FRET between the dye pair (Rao et al., 2016). While we observed rapid TA transfer from Sgt2 to wild-type Get3 in the presence of Get4/5 (see also (Rao et al., 2016)), TA transfer to Get3(Δα8) under the same conditions was ~100-fold slower (Figure 2C). Therefore, α8 plays an important role in ensuring rapid TA transfer from Sgt2 to Get3.

Since the Get4/5 complex also stimulates TA transfer from Sgt2 to Get3 (Mateja et al., 2015; Rao et al., 2016; Wang et al., 2010), we asked whether Get4/5 and α8 work synergistically or independently of one another. We therefore measured and compared the rate of TA transfer from Sgt2 to Get3 and Get3(Δα8) without Get4/5 present. Without Get4/5, deletion of α8 has a less deleterious effect, slowing TA transfer kinetics 12-fold (Figures 2D and 2E). Reciprocally, Get4/5 exerts a smaller stimulatory effect on the Sgt2-to-Get3 TA transfer with mutant Get3(Δα8) compared to wild-type Get3 (Figure 2E, last row). In control experiments, Get3(Δα8) binds Get4/5 and undergoes Get4/5-induced conformational changes similarly to wild-type Get3 (Figures S2E–F and S3), ruling out the possibility that the defect of Get3(Δα8) in Get4/5-dependent TA transfer is due to its defective binding or regulation by Get4/5. Together, these results show that α8 and Get4/5 synergistically enhance TA transfer from Sgt2 to Get3.

Previously, it was shown that TA transfer from SGTA to TRC40, the respective mammalian homologs of Sgt2 and Get3, was impervious to the presence of excess CaM (Shao et al., 2017). We asked if α8 is important for maintaining this ‘privileged’ transfer. To this end, we repeated the FRET-based TA transfer assay in the presence of excess CaM (Figure 3). TA transfer from Sgt2 to wild-type Get3•Get4/5 was not affected by excess CaM (Figure 3B), consistent with observations with their mammalian homologues. In contrast, the presence of CaM completely abolished FRET between TA and Get3 in transfer reactions without Get4/5 present (Figure 3C), or with mutant Get3(Δα8) even in the presence of Get4/5 (Figure 3D). Thus, TA transfer to Get3 becomes susceptible to interference by external chaperones in the absence of either Get4/5 or the α8 motif.

To independently test this model, we monitored the Sgt2-to-Get3 TA transfer using a crosslinking assay. Instead of a fluorescent dye, the photocrosslinker p-benzoyl-l-phenylalanine (Bpa) was incorporated into the TA-TMD via amber suppression (Young et al., 2010). UV-induced crosslinking to Bpa allows direct visualization of the interaction of TA with different chaperones via SDS-PAGE and autoradiography (Figure 3F). In the absence of Get3, TA was rapidly lost from Sgt2 and transferred to CaM (Figure 3H), as was observed with the SGTA•TA complex (Shao et al., 2017). Addition of Get3•Get4/5 resulted in rapid transfer of TA to Get3 without any TA loss to CaM (Figure 3G), consistent with observations for the homologous mammalian transfer complex (Shao et al., 2017) and with

results of the FRET measurements (Figure 3B). In contrast, TA transfer to Get3(Δα8)•Get4/5 was almost completely abolished by the presence of CaM, and most of the TA crosslinked to CaM instead (Figure 3I). Together, the FRET and crosslinking experiments demonstrate that the α8 motif plays an essential role in enabling privileged TA transfer between Sgt2 and Get3.

Lastly, we tested whether the role of α8 in the Sgt2-to-Get3 TA transfer explains the defect of Get3(Δα8) in the overall targeting reaction (Figure S1D). To this end, we initiated TA targeting by mixing a preformed Sgt2•TA complex with Get3, Get4/5, and yRM (Figure 4A), such that the observed insertion reaction includes the TA transfer step. Addition of wild-type Get3 led to robust TA insertion within 5 min, whereas negligible insertion was observed with Get3(Δα8) (Figure 4A). This contrasts with the absence of a targeting defect with the preformed Get3(Δα8) complex (Figure 2A) and indicates that the defect of Get3(Δα8) can be attributed to the loss of efficient TA transfer from Sgt2 to Get3.

Discussion

Molecular chaperones play key roles in membrane protein biogenesis. While guiding client proteins to the target membrane, these chaperones must effectively secure hydrophobic TMDs on client proteins to prevent both aggregation and client loss to off-pathway chaperones. These challenges are especially acute for pathways in which client proteins undergo molecular handovers between chaperones. In this work, biochemical and biophysical analyses shed light on how a conserved α8 lid motif lining the substrate binding groove enables the Get3 ATPase to fulfill these requirements during TA targeting to the ER.

The importance of the α8 element is supported by its evolutionary conservation among Get3 homologues (Figure S1) (Mateja et al., 2009; Suloway et al., 2009), yeast growth defects under stress conditions upon mutation of α8 (Mateja et al., 2009), and the defects of mutant Get3(Δα8) in TA targeting *in vitro* and *in vivo* (this work). However, the precise roles of α8 remained enigmatic. Mechanistic dissections in this work show that the major roles of α8 are to accelerate TA transfer to Get3 from the upstream co-chaperone Sgt2 and to confer upon Get3 the privilege to receive TAs over competing chaperones. Deletion of hydrophobic residues in α8 slowed Get4/5-dependent TA transfer from Sgt2 to Get3 by ~100-fold (Figures 2C and 2E). Moreover, Get3 lost its privilege in capturing TAs from Sgt2 upon mutation of α8, and the TA substrate can be rapidly lost to an external chaperone (Figure 3). This explains the previous observation that mutations in α8 reduced the amount of Get3-bound TAs in pulldown assays in rabbit reticulocyte lysate (Mateja et al., 2009). The cooperative effects of Get4/5 and α8 in promoting rapid and privileged TA transfer further suggest that they both stabilize the transition state or a transient intermediate during the transfer reaction. Coupled with the observation that α8 can crosslink to the TA (Mateja et al., 2015), the simplest model to explain all the data is that α8 provides the first structural element in Get3 to contact the TA during its handover from Sgt2, guiding the TA into the hydrophobic substrate binding groove of Get3 and protecting the TA from off-pathway chaperones during this process (Figure 4B, bracket).

Once the TA is loaded onto Get3, deletion of α8 also renders the TA more susceptible to challenges by external TMD-binding chaperones (Figure 4B). Whether TAs could be analogously lost from Get3(Δα8) to other chaperones in the yeast cytosol remains to be determined. Nevertheless, the observation here that two unrelated membrane protein chaperones, cpSRP43 and CaM, can both invade the TA binding groove and capture TAs from Get3(Δα8) suggest that loss of substrates to off-pathway chaperones presents a probable mechanistic challenge during membrane protein biogenesis, and that some chaperones such as Get3 have evolved mechanisms to actively retain substrates within the dedicated targeting pathway.

The role of the α8 lid motif in facilitating rapid and privileged TA loading onto the chaperone is unprecedented, and highlights new mechanistic challenges as well as solutions for molecular chaperones. A dual-function lid described here provides an effective and elegant mechanism for a chaperone to capture and retain client proteins within the correct biogenesis pathway during and after substrate handover. This function may be particularly relevant for chaperones that interact with client proteins via degenerate interactions and face competition from other chaperones in the crowded cytosolic environment.

STAR★ METHODS

CONTACT FOR REAGENT AND RESOURCE SHARING

Further information and requests for resources and reagents should be directed to and will be fulfilled by the Lead Contact, Shu-ou Shan (sshan@caltech.edu).

EXPERIMENTAL MODEL AND SUBJECT DETAILS

***S. cerevisiae* strains—**All *S. cerevisiae* strains used in this study are listed in the Key Resources Table.

***S. cerevisiae* strain construction—**Genomic *GET3* in the BY4741 strain was replaced with *GET3-FLAG* and *GET3(Δα8)-FLAG* using CRISPR-Cas9 mediated genome editing (Ryan et al., 2016). The pCAS plasmid encoding *S. pyogenes* Cas9 and sgRNA was modified to encode a guide sequence (5'-GAATATAACCCTATTACTGA-3') that targets Cas9 to cut the codon for Get3(T342). This pCAS plasmid was co-transformed into BY4741 yeast cells with a double-stranded linear repair DNA, which encodes Get3-FLAG harboring synonymous codon substitutions within the guide sequence and 50 bp homology downstream of the C-terminal FLAG tag for homologous recombination. The *GET3(Δα8)-FLAG* strain was then generated using a modified pCAS plasmid encoding a guide sequence (5'-GTTGTAGAAATCTTAATGTG-3') that targets Cas9 to cut the codon for Get3(T173). The modified pCAS was co-transformed with a double-stranded linear repair DNA that encodes Get3(Δα8)-FLAG with synonymous codon substitutions within the guide sequence into *GET3-FLAG* yeast cells. Following each co-transformation, colonies from the YPD +G418 plate were cultured in YPD, streaked onto YPD, and cultured again in YPD to ensure loss of the pCAS plasmid. The final strains were verified by PCR and sequencing.

METHOD DETAILS

Plasmids and recombinant proteins—All plasmids and recombinant proteins used in this study are listed in the Key Resources Table. All proteins and protein complexes were ultracentrifuged (TLA100, Beckman Coulter Inc.) at 100,000 rpm for 30 min at 4 °C to remove potential aggregates prior to use in *in vitro* assays.

Protein labeling—Get3 and Get3(Δα8) with a ybbR tag (DSLEFIASKLA) inserted between residues S110 and D111 were labeled with BODIPY-FL (Thermo Fisher Scientific) or a 1:1 mix of Cy3B (GE Healthcare) and ATTO 647N (ATTO-TEC) via Sfp-catalyzed incorporation of dye-CoA conjugates (Rao et al., 2016). 30 μM ybbR-Get3 was mixed with 60 μM dye-CoA and 12 μM Sfp-His_6 in Sfp labeling buffer (50 mM K-HEPES (pH 7.4), 10 mM $MgCl_2$) in a total volume of 800 μL. The reaction mixture was rotated at room temperature for 1 hr. 10 μL 2 M imidazole (pH 8.0) was added before passing the reaction through Ni-NTA agarose (Qiagen) to remove Sfp-His_6. Gel filtration through a Sephadex G-25 (Sigma-Aldrich) column was used to remove excess dye-CoA and exchange dye-labeled Get3 into GET storage buffer (50 mM K-HEPES (pH 7.5), 150 mM KOAc, 5 mM $Mg(OAc)_2$, 20% glycerol, 1 mM DTT).

Get4(C177T/S48C)/5 was labeled with thiol-reactive acrylodan (Thermo Fisher Scientific) (Rome et al., 2014). Protein was dialyzed into labeling buffer (50 mM K-HEPES (pH 7.4), 200 mM NaCl, 10% glycerol) and treated with 2 mM TCEP to reduce disulfide bonds. A 10-fold excess of acrylodan was added and the reaction was incubated overnight at 4°C. The reaction was quenched with 1 mM DTT and excess dye was removed using a Sephadex G-25 column while exchanging acrylodan-labeled Get4/5 into GET storage buffer.

TA substrate was labeled either four residues upstream of the TMD with 7-hydroxycoumarin or replacing Ala 228 in Bos1 TMD with p-benzoyl-l-phenylalanine (Bpa) using amber suppression in *E. coli* S30 lysate (Rao et al., 2016; Young et al., 2010).

Model TA substrates—The model TA used in all *in vitro* assays was the previously described 3xStrep-SUMOnc-Bos1-opsin (Rao et al., 2016), composed of three tandem Strep tags at the N-terminus, a mutant yeast Smt3 with the Ulp1 cut site removed (Pro inserted between residues G98 and A99), the C-terminal residues 207–244 of the TA Bos1 encompassing its TMD, and an opsin tag at the extreme C-terminus (GSMRMNGTEGPNMYMPMSNKTVD) to monitor ER translocation via glycosylation. The model TA for *in vivo* pulse chase experiments was 3xHA-BirA-Bos1TMD-opsin (Cho and Shan, 2018), composed of an N-terminal 3xHA-BirA for HA immunoprecipitation, the C-terminal residues 203–244 of the TA Bos1 encompassing its TMD, a GS linker (GSGGSGS), and an opsin tag at the extreme C-terminus.

Get3•TA and Sgt2•TA complex preparation—For fluorescence measurements, $Get3^{BDP}$•TA^{CM} complexes were generated by *in vitro* translating 3xStrep-tagged TA^{CM} for 2 hrs at 30°C in 10 mL amber suppression reactions with *E. coli* S30 lysate in the presence of 0.5 μM BODIPY-FL-labeled Get3 variants. For insertion assays, 3xStrep-tagged TA was *in vitro* translated for 2 hrs at 30 □ in a 100 μL reaction with *E. coli* S30 lysate in the

presence of 2 μM Get3 variants. The resulting Get3•TA complexes were then purified using Strep-Tactin Sepharose (IBA Life Sciences).

Sgt2•TA complexes for transfer and insertion assays were generated by *in vitro* translation of TA^{CM}, TA(Bpa), or TA for 2 hrs at 30 °C in 10 mL or 100 μL amber suppression reactions with *E. coli* S30 lysate in the presence of 1 μM His_6-tagged Sgt2. The Sgt2•TA complex was then purified using Ni-NTA (Qiagen).

Fluorescence measurements of Get3•TA dissociation—All fluorescence measurements were carried out on a Fluorolog 3–22 spectrophotometer (HORIBA Instruments) at 25 °C in GET assay buffer (50 mM K-HEPES (pH 7.4), 150 mM KOAc, 5 mM $Mg(OAc)_2$, 10% glycerol, 1 mM DTT).

Get3•TA dissociation rates were measured by chasing 20–50 nM of preformed $Get3^{BDP}$•TA^{CM} complexes with indicated concentrations of intein-cpSRP43 or CaM. Loss of FRET over time was monitored by following the fluorescence of TA^{CM} using an excitation wavelength of 370 nm and emission wavelength of 450 nm. Observed time courses were fit to Equation 1:

$$F = F_e + (F_0 - F_e)e^{-k_{obsd}t} \quad (1)$$

where F is the observed donor fluorescence at a particular time, F_0 is the donor fluorescence at t=0, F_e is the donor fluorescence when the reaction is complete, and k_{obsd} is the observed rate constant of TA loss from Get3.

Kinetic simulations of Get3•TA dissociation—Kinetic simulations for the different models of Bos1-TA release from Get3(Δα8) were performed with Berkeley Madonna, version 8.3.18 (R. I. Macey, G. F. Oster, University of California at Berkeley). For the passive model (Figure 1G), the following equations were used:

$$\text{Get3}(\Delta\alpha8) \bullet \text{TA} \underset{k_{-1}}{\overset{k_1}{\rightleftharpoons}} \text{Get3}(\Delta\alpha8) + \text{TA} \quad (2)$$

$$\text{TA} + \text{cpSRP43} \underset{k_{-2}}{\overset{k_2}{\rightleftharpoons}} \text{cpSRP43} \bullet \text{TA} \quad (3)$$

For the active model (Figure 1H), the following chemical equations were used:

$$\text{Get3}(\Delta\alpha8) \bullet \text{TA} \underset{k_{-1}}{\overset{k_1}{\rightleftharpoons}} \text{Get3}(\Delta\alpha8) + \text{TA} \quad (2)$$

$$\text{TA} + \text{cpSRP43} \underset{k_{-2}}{\overset{k_2}{\rightleftharpoons}} \text{cpSRP43} \bullet \text{TA} \quad (3)$$

$$\text{Get3}(\Delta\alpha 8) \bullet \text{TA} + \text{cpSRP43} \underset{k_{-3}}{\overset{k_3}{\rightleftharpoons}} \text{Get3}(\Delta\alpha 8) + \text{cpSRP43} \bullet \text{TA} \quad (4)$$

The rate constant k_1 was experimentally determined to be 0.0026 min^{-1}, or 4.3×10^{-5} s^{-1} (Figure 1F). The K_d value of wild-type Get3•Bos1-TA was estimated to be 0.1 nM based on the coupled equilibria of TA loading and transfer through the Ssa1-Sgt2-Get3 cascade (Cho and Shan, 2018; Rao et al., 2016) shown in Equation 5:

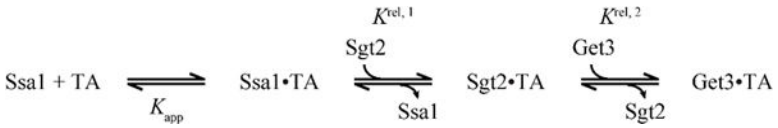

(5)

The Ssa1 concentration required for half-maximal solubilization of Bos1-TA (K_{app}) was previously determined to be 0.37 ± 0.07 μM (Cho and Shan, 2018). Equilibrium titrations of Bos1-TA transfer from Ssa1 to Sgt2 indicated that this first transfer reaction is ~100-fold in favor of Sgt2 ($K^{rel,1} \sim 100$) (Cho and Shan, 2018). Equilibrium titrations of Bos1-TA transfer from Sgt2 to Get3 suggested that this second transfer reaction is ~30-fold in favor of Get3 ($K^{rel,2} \sim 30$) (Rao et al., 2016). These data provide estimated K_d values of Sgt2•Bos1-TA and Get3•Bos1-TA of approximately 3.7 nM and 0.1 nM, respectively. This K_d and the measured k_1 value yield a calculated k_{-1} of approximately 4.3×10^5 $M^{-1}s^{-1}$ for wild-type Get3•TA. Given the 100-fold slower $k_{transfer}$ of Get3(Δα8) than wild-type Get3 (Figure 2), we estimated a 100-fold lower value of k_{-1}, 4.3×10^3 M^{-1} s^{-1}, for Bos1-TA binding to Get3(Δα8). Variations in the value of k_{-1} did not change the qualitative conclusion that the observed rate constant of Bos1-TA loss from Get3(Δα8) is independent of chase concentration in the passive model (Figures S4E and S4F).

From chase experiments of wild-type Get3•Bos1-TA with cpSRP43, we found that a cpSRP43 concentration of 21 ± 0.7 μM was necessary for half-maximal Bos1-TA transfer in the presence of 50 nM Get3 after fitting the data in Figure S4B to:

$$F = F_{max} \times \frac{[\text{cpSRP43}]}{K_{1/2,app} + [\text{cpSRP43}]} \quad (6)$$

This strongly suggests that intein-cpSRP43 binds TA with an ~400-fold weaker affinity than Get3. We estimated a K_d of ~40 nM for the cpSRP43-TA interaction. We assigned a lower limit for k_2 of 1×10^5 M^{-1} s^{-1}, given the observation that TA aggregation occurs within the

mixing dead-time of ~15 s and that intein-cpSRP43 effectively competes with TA aggregation (Cho and Shan, 2018). k_{-2} was calculated to be 0.004 s^{-1} from the estimated K_d and k_2 values. Increasing the values of k_2 and k_{-2} (holding a constant K_d value) does not change the results of the simulation (Figures S4G and S4H).

Normalized fluorescence change is proportional to the loss of the Get3(Δα8)•Bos1-TA complex and was calculated as:

$$F = 1 - \frac{[\text{Get3}(\Delta\alpha8) \bullet \text{TA}]}{[\text{Get3}(\Delta\alpha8) \bullet \text{TA}]_0} \quad (7)$$

where $[\text{Get3}(\Delta\alpha8)\bullet\text{TA}]_0$ is the initial Get3(Δα8)•TA concentration and was set to 20 nM. The rate constants k_3 and k_{-3} in Equation 4 were determined to be 1.54×10^3 M^{-1} min^{-1} and 5.11×10^{-4} min^{-1}, respectively, by allowing the software to fit the simulated time courses to the experimental results. The obtained value of k_3 was equal to that obtained from manual fitting of the data in Figure 1B, which was also 1.54×10^3 M^{-1} min^{-1}.

Monitoring TA transfer from Sgt2 to Get3—TA^{CM} transfer from Sgt2 to $Get3^{BDP}$ was monitored by mixing 120 μL of ~50 nM Sgt2• TA^{CM} with 120 μL of a solution containing 0.6 μM or 6 μM $Get3^{BDP}$. 2 mM ATP was present in all reactions. Where indicated, transfer reactions also contained 0.15 μM Get4/5 with and without 40 μM CaM (supplemented with 1 mM Ca^{2+}). To correct for photobleaching and possible environmental effects on the donor fluorophore, transfer reactions to unlabeled Get3 were also performed in parallel under the same conditions. Time courses of fluorescence changes were recorded for TA^{CM}, corrected for photobleaching and possible environmental effects, and fit to Equation 1, where k_{obsd} is the observed rate constant for TA transfer from Sgt2 to Get3.

To monitor TA transfer from Sgt2 to Get3 via crosslinking, Sgt2•TA(Bpa), containing 300 nM Sgt2 and sub-stoichiometric levels of [^{35}S]-methionine-labeled TA(Bpa), was added to 750 nM Get3 and 750 nM Get4/5. Where indicated, CaM was present at 20 μM. All reactions contained 2 mM ATP, 1 mM Ca^{2+} and were incubated at 26 °C. At indicated time points, aliquots were removed from the reaction, flash frozen, and subsequently crosslinked on dry ice ~4 cm away from a UVP B-100AP lamp (UVP LLC) for 90 minutes. Aliquots were then thawed and processed for SDS-PAGE and autoradiography.

TA targeting assays—To monitor TA targeting and translocation from preformed Get3•TA or Get3(Δα8)•TA complexes, 50 μL reactions were initiated by adding 10 μL *Δget3* microsomes to purified Get3•TA complexes in the presence of 0.5 μM Get4/5 and 2 mM ATP. [^{35}S]-methionine-labeled TA was normalized to 40,000 dpm for each reaction. Reactions were incubated at 26 °C; at indicated time points, 6 μL samples were removed and quenched by addition of SDS sample buffer and flash-freezing in liquid nitrogen. Samples were analyzed by SDS-PAGE and autoradiography. Insertion efficiencies were calculated using Equation 2:

$$Insertion\ \ efficiency = \frac{I_{glycosylated}}{I_{unglycosylated} + I_{glycosylated}} \times 100 \quad (8)$$

where I denotes the intensity of the band of interest.

TA targeting and insertion assays starting with a preformed Sgt2•TA complex were measured using purified Sgt2•TA complexes, in which TA is ^{35}S-methionine labeled and normalized to 40,000 dpm. Sgt2•TA was first mixed with other components except for microsomes to 8 μL, and then after 15s, 2 μL *Δget3* microsomes were added to initiate reactions. Reactions contained 75 nM Get4/5, 2 mM ATP, 0.5 μM wild-type Get3 or Get3(Δα8), and 20 μM cpSRP43 where indicated. Initiated reactions were incubated at 26 °C for 5 minutes before quenching with SDS sample buffer and flash freezing with liquid nitrogen. Samples were analyzed by SDS-PAGE and autoradiography. Insertion efficiencies were calculated using Equation 8.

Pulse-chase analysis of TA insertion in vivo—*GET3-FLAG*, *GET3(Δα8)-FLAG,* and *Δget3* yeast cells were first transformed with a pRS316 vector containing a GPD promoter and the 3xHA-BirA-Bos1TMD-opsin TA substrate (Cho and Shan, 2018). Transformed yeast cells were grown in SD-Ura to mid-log phase (OD_{600} ~ 0.6), washed with SD-Ura-Met-Cys media, and resuspended in 1 mL SD-Ura-Met-Cys media to a final OD_{600} of 6. Cells were incubated at 30 °C for 25 min and then incubated at 26 °C for an additional 10 min. Cells were pulse-labeled with 100 μCi/mL EasyTag™ EXPRESS35S Protein Labeling Mix (Perkin Elmer) for 2 min and chased with 1 mL SD-Ura supplemented with 20 mM cold methionine and 2 mM cysteine. 450 μL aliquots of cells were flash frozen in liquid nitrogen at indicated times during chase. Individual cell aliquots were subsequently thawed and harvested.

Cells were treated with 0.3 M NaOH for 3 min at room temperature, washed with water, resuspended in Lysis buffer (20 mM Tris-HCl (pH 7.6), 150 mM NaCl, 2% SDS), incubated at 70 °C for 10 min, and then spun down at 14,000 rpm (16,873 g) for 2 min. Clarified lysate was diluted over 20-fold with HA IP buffer (20 mM Tris-HCl (pH 7.6), 150 mM NaCl, 1% Triton X-100) and incubated with anti-HA magnetic beads (Thermo Fisher Scientific) equilibrated with HA IP buffer containing 0.4 mg/mL BSA. After incubation at 25 °C for 10 min, the beads were sequentially washed with: W1 buffer (20 mM Tris-HCl (pH 7.6), 150 mM NaCl, 1% Triton X-100, 2M urea), W2 buffer (20 mM Tris-HCl (pH 7.6), 500 mM NaCl, 1% Triton X-100), W3 buffer (20 mM Tris-HCl (pH 7.6), 150 mM NaCl, 0.1% SDS), and W4 buffer (20 mM Tris-HCl (pH 7.6), 150 mM NaCl). The final wash with W4 buffer was performed twice. Immunoprecipitated proteins were eluted with SDS sample buffer, boiled for 5 min, and analyzed by SDS-PAGE and autoradiography. Insertion efficiencies were calculated using Equation 8.

Circular dichroism—Circular dichroism spectra of wild-type Get3 or Get3(Δα8) at 5 μM in 20 mM sodium phosphate pH 7.5 were recorded using an Aviv Model 430 circular

dichroism spectrometer at 25 °C. For each sample, 8 scans from 190 nm to 260 nm were collected, averaged, and background subtracted.

ATPase measurements—Multi-site, multi-turnover ATPase rate constants were measured for 0.5 μM Get3(Δα8) and indicated ATP concentrations in GET assay buffer at 25 °C (Rome et al., 2013). The ATP concentration dependence of observed rate constants were fit to an allosteric sigmoidal curve with a Hill coefficient of 2 (Equation 9):

$$k_{obsd} = \frac{k_{cat} \times [ATP]^2}{K_M^2 + [ATP]^2} \quad (9)$$

where k_{cat} is the rate constant at saturating ATP concentrations, and K_M^2 is the product of ATP binding affinities for the first and second active site.

Measurements of Get3-Get4/5 binding—Equilibrium binding affinities between Get3 variants and acrylodan-labeled Get4/5 were measured by titrating 250 μL of 0.5 μM acrylodan-labeled Get4/5 with increasing Get3 concentration in the absence (Figure S2E) or presence (Figure S2F) of 2 mM ATP. Binding of Get3 results in fluorescence enhancement of acrylodan-labeled Get4/5 and was recorded using an excitation wavelength of 370 nm and emission wavelength of 490 nm. Fluorescence was plotted against Get3 concentration and fit to Equation 10:

$$F = F_0 + F_{max} \times \frac{K_d + [Get4/5] + [Get3] - \sqrt{(K_d + [Get3] + [Get4/5])^2 - 4[Get3][Get4/5]}}{2[Get4/5]} \quad (10)$$

where F is the observed fluorescence, F_0 is the initial fluorescence value, F_{max} is the maximum fluorescence change at saturating Get3 concentration, and K_d is the equilibrium dissociation constant of the complex.

μs-ALEX measurements—All proteins were ultracentrifuged in a TLA 100 rotor (Beckman Coulter) at 100,000 rpm for 1 hr at 4 °C to remove aggregates before all measurements. Get3 samples were diluted to ~100 pM in GET assay buffer containing 0.3 mg/mL BSA and indicated interaction partners. 2 mM AMPPNP, 4 mM ADP, 10 μM Get1CD, and 4 μM Get4/5 were included where indicated. Samples were placed in a closed chamber made by sandwiching a perforated silicone sheet (Grace Bio-Labs) with two coverslips to prevent evaporation. Data were collected over 30 min using an alternating-laser excitation fluorescence-aided molecule sorting setup (Kapanidis et al., 2004) with two single-photon Avalanche photodiodes (PerkinElmer) and 532-nm and 638-nm continuous wave lasers (Coherent) operating at 135 μW and 80 μW, respectively.

QUANTIFICATION AND STATISTICAL ANALYSIS

Statistical parameters—All statistical parameters (n and SD) for assays in this study are reported in the corresponding figure legends.

μs-ALEX data analysis—For the collected μs-ALEX data, a dual-channel burst search (Nir et al., 2006) was performed using FRETBursts (Ingargiola et al., 2016) to isolate the photon streams from species containing FRET pairs versus background noise and species containing donor or acceptor only. Each burst was identified as a minimum of 10 consecutive detected photons with a photon count rate at least 15-fold higher than the background photon count rate during both donor and acceptor excitation periods. Since the background rate can fluctuate within a measurement, the background rate was computed for every 50-s interval according to maximum likelihood fitting of the interphoton delay distribution. The identified bursts were further selected according to the following criteria: (i) $n_{DD} + n_{DA} \geq 25$ and (ii) $n_{AA} \geq 25$, where n_{DD} is the number of photons detected from donor during donor excitation, n_{DA} is the number of photons detected from acceptor during donor excitation, and n_{AA} is the number of photons detected from acceptor during acceptor excitation.

Supplementary Material

Refer to Web version on PubMed Central for supplementary material.

Acknowledgements

We thank J. Chartron for advice on generating yeast strains using CRISPR-Cas9; R.S. Hegde for CaM expression vectors; H. Cho, M. Rao, F. Liang, A. Siegel, and S. Wang for reagents; S. Hematian and the Beckman Institute Laser Resource Center for training and use of circular dichroism spectrometer; M. Rao for initial observations; and members of the Shan laboratory for critical discussions and comments on the manuscript. This work was supported by Dean Willard Chair funds to S.W. and NIH grant GM107368, Gordon and Betty Moore Foundation Grant GBMF2939, and fellowship from the Weston Havens foundation to S.-o.S.

References

Akopian D, Shen K, Zhang X, and Shan S-O (2013). Signal recognition particle: an essential protein-targeting machine. Annu. Rev. Biochem. 82, 693–721. [PubMed: 23414305]

Burmann BM, Wang C, and Hiller S (2013). Conformation and dynamics of the periplasmic membrane-protein-chaperone complexes OmpX-Skp and tOmpA-Skp. Nat. Struct. Mol. Biol. 20, 1265–1272. [PubMed: 24077225]

Chartron JW, Suloway CJM, Zaslaver M, and Clemons WM (2010). Structural characterization of the Get4/Get5 complex and its interaction with Get3. Proc. Natl. Acad. Sci. U. S. A. 107, 12127–12132. [PubMed: 20554915]

Chio US, Cho H, and Shan S-O (2017a). Mechanisms of tail-anchored membrane protein targeting and insertion. Annu. Rev. Cell Dev. Biol. 33, 417–438. [PubMed: 28992441]

Chio US, Chung S, Weiss S, and Shan S-O (2017b). A protean clamp guides membrane targeting of tail-anchored proteins. Proc. Natl. Acad. Sci. 114, E8585–E8594. [PubMed: 28973888]

Cho H, and Shan S-O (2018). Substrate relay in an Hsp70-cochaperone cascade safeguards tail-anchored membrane protein targeting. EMBO J. e99264.

Gristick HB, Rao M, Chartron JW, Rome ME, Shan S-O, and Clemons WM (2014). Crystal structure of ATP-bound Get3-Get4-Get5 complex reveals regulation of Get3 by Get4. Nat. Struct. Mol. Biol. 21, 437–442. [PubMed: 24727835]

Gristick HB, Rome ME, Chartron JW, Rao M, Hess S, Shan S-O, and Clemons WM (2015). Mechanism of assembly of a substrate transfer complex during tail-anchored protein targeting. J. Biol. Chem. 290, 30006–30017. [PubMed: 26451041]

Hegde RS, and Keenan RJ (2011). Tail-anchored membrane protein insertion into the endoplasmic reticulum. Nat. Rev. Mol. Cell Biol. 12, 787–798. [PubMed: 22086371]

Hu J, Li J, Qian X, Denic V, and Sha B (2009). The crystal structures of yeast Get3 suggest a mechanism for tail-anchored protein membrane insertion. PLoS One 4, e8061.

Huang C, Rossi P, Saio T, and Kalodimos CG (2016). Structural basis for the antifolding activity of a molecular chaperone. Nature 537, 202–206. [PubMed: 27501151]

Ingargiola A, Lerner E, Chung S, Weiss S, and Michalet X (2016). FRETBursts: an open source toolkit for analysis of freely-diffusing single-molecule FRET. PLoS One 11, e0160716.

Jaru-Ampornpan P, Shen K, Lam VQ, Ali M, Doniach S, Jia TZ, and Shan S-O (2010). ATP-independent reversal of a membrane protein aggregate by a chloroplast SRP subunit. Nat. Struct. Mol. Biol. 17, 696–702. [PubMed: 20424608]

Kapanidis AN, Lee NK, Laurence TA, Doose S, Margeat E, and Weiss S (2004). Fluorescence-aided molecule sorting: analysis of structure and interactions by alternating-laser excitation of single molecules. Proc. Natl. Acad. Sci. U. S. A. 101, 8936–8941. [PubMed: 15175430]

Kim YE, Hipp MS, Bracher A, Hayer-Hartl M, and Ulrich Hartl F (2013). Molecular chaperone functions in protein folding and proteostasis. Annu. Rev. Biochem. 82, 323–355. [PubMed: 23746257]

Liang F-C, Kroon G, McAvoy CZ, Chi C, Wright PE, and Shan S-O (2016). Conformational dynamics of a membrane protein chaperone enables spatially regulated substrate capture and release. Proc. Natl. Acad. Sci. 113, E1615–E1624. [PubMed: 26951662]

Mateja A, Szlachcic A, Downing ME, Dobosz M, Mariappan M, Hegde RS, and Keenan RJ (2009). The structural basis of tail-anchored membrane protein recognition by Get3. Nature 461, 361–366. [PubMed: 19675567]

Mateja A, Paduch M, Chang H, Szydlowska A, Kossiakoff AA, Hegde RS, and Keenan RJ (2015). Structure of the Get3 targeting factor in complex with its membrane protein cargo. Science 347, 1152–1155. [PubMed: 25745174]

Mayer MP, and Bukau B (2005). Hsp70 chaperones: cellular functions and molecular mechanism. Cell. Mol. Life Sci. 62, 670–684. [PubMed: 15770419]

Nir E, Michalet X, Hamadani KM, Laurence TA, Neuhauser D, Kovchegov Y, and Weiss S (2006). Shot-noise limited single-molecule FRET histograms: comparison between theory and experiments. J. Phys. Chem. B 110, 22103–22124. [PubMed: 17078646]

Rao M, Okreglak V, Chio US, Cho H, Walter P, and Shan S-O (2016). Multiple selection filters ensure accurate tail-anchored membrane protein targeting. Elife 5, e21301. [PubMed: 27925580]

Rome ME, Rao M, Clemons WM, and Shan S-O (2013). Precise timing of ATPase activation drives targeting of tail-anchored proteins. Proc. Natl. Acad. Sci. U. S. A. 110, 7666–7671. [PubMed: 23610396]

Rome ME, Chio US, Rao M, Gristick HB, and Shan S-O (2014). Differential gradients of interaction affinities drive efficient targeting and recycling in the GET pathway. Proc. Natl. Acad. Sci. U. S. A. 111, E4929–E4935. [PubMed: 25368153]

Ryan OW, Poddar S, and Cate JHD (2016). CRISPR–Cas9 genome engineering in Saccharomyces cerevisiae cells. Cold Spring Harb. Protoc. 2016, pdb.prot086827.

Saraogi I, Zhang D, Chandrasekaran S, and Shan S-O (2011). Site-specific fluorescent labeling of nascent proteins on the translating ribosome. J. Am. Chem. Soc. 133, 14936–14939. [PubMed: 21870811]

Schuenemann D, Gupta S, Persello-Cartieaux F, Klimyuk VI, Jones JD, Nussaume L, and Hoffman NE (1998). A novel signal recognition particle targets light-harvesting proteins to the thylakoid membranes. Proc. Natl. Acad. Sci. 95, 10312–01316. [PubMed: 9707644]

Schuldiner M, Collins SR, Thompson NJ, Denic V, Bhamidipati A, Punna T, Ihmels J, Andrews B, Boone C, Greenblatt JF, et al. (2005). Exploration of the function and organization of the yeast early secretory pathway through an epistatic miniarray profile. Cell 123, 507–519. [PubMed: 16269340]

Schuldiner M, Metz J, Schmid V, Denic V, Rakwalska M, Schmitt HD, Schwappach B, and Weissman JS (2008). The GET complex mediates insertion of tail-anchored proteins into the ER membrane. Cell 134, 634–645. [PubMed: 18724936]

Shao S, and Hegde RS (2011). A calmodulin-dependent translocation pathway for small secretory proteins. Cell 147, 1576–1588. [PubMed: 22196732]

Shao S, Rodrigo-Brenni MC, Kivlen MH, and Hegde RS (2017). Mechanistic basis for a molecular triage reaction. Science 355, 298–302. [PubMed: 28104892]

Stefanovic S, and Hegde RS (2007). Identification of a targeting factor for posttranslational membrane protein insertion into the ER. Cell 128, 1147–1159. [PubMed: 17382883]

Suloway CJM, Chartron JW, Zaslaver M, and Clemons WM (2009). Model for eukaryotic tail-anchored protein binding based on the structure of Get3. Proc. Natl. Acad. Sci. U. S. A. 106, 14849–14854. [PubMed: 19706470]

Thoma J, Burmann BM, Hiller S, and Müller DJ (2015). Impact of holdase chaperones Skp and SurA on the folding of β-barrel outer-membrane proteins. Nat. Struct. Mol. Biol. 22, 795–802. [PubMed: 26344570]

Wang F, Brown EC, Mak G, Zhuang J, and Denic V (2010). A chaperone cascade sorts proteins for posttranslational membrane insertion into the endoplasmic reticulum. Mol. Cell 40, 159–171. [PubMed: 20850366]

Yin J, Lin AJ, Golan DE, and Walsh CT (2006). Site-specific protein labeling by Sfp phosphopantetheinyl transferase. Nat. Protoc. 1, 280–285. [PubMed: 17406245]

Young TS, Ahmad I, Yin JA, and Schultz PG (2010). An enhanced system for unnatural amino acid mutagenesis in *E. coli*. J. Mol. Biol. 395, 361–374. [PubMed: 19852970]

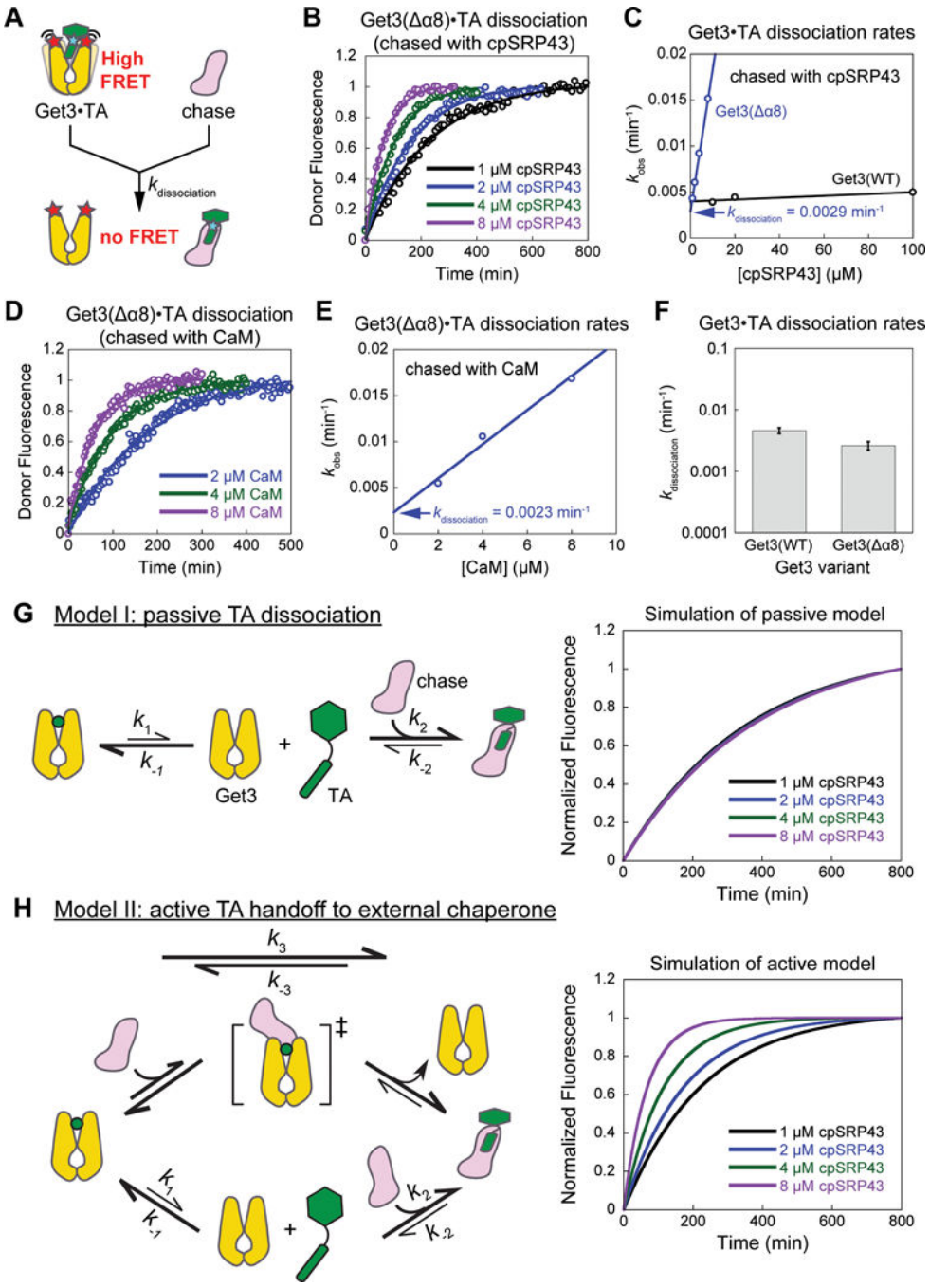

Figure 1.

α8 prevents promiscuous TA handoff from Get3 to off-pathway chaperones.

(A) Schematic for measurement of Get3•TA dissociation kinetics. TA was labeled with a donor dye (cyan star), and Get3 was labeled with acceptor dyes (red stars). Addition of a chase drives irreversible Get3•TA dissociation, which can be monitored as a loss of FRET over time.

(B), (D) Time courses for change in the fluorescence of TA^{CM} to monitor TA loss from Get3(Δα8) (50 nM initial complex) using indicated concentrations of intein-cpSRP43 (B) or

CaM (D) as chase. Fluorescence was normalized such that the fit of each trace starts at 0 and ends at 1.

(C), (E) Increasing concentrations of intein-cpSRP43 (C) or CaM (E) accelerated the observed rate of TA loss from Get3(Δα8), but not from wild-type Get3.

(F) Summary of the dissociation rate constants for Get3•TA and Get3(Δα8)•TA complexes (0.0044 ± 0.0006 and 0.0026 ± 0.0004 min^{-1}, respectively). Error bars denote SD, with n = 2–3.

(G) Kinetic simulations (right) based on the passive model (left schematic), in which TA is first released from Get3(Δα8) before binding the chase.

(H) Kinetic simulations (right) based on the active model (left schematic), in which Get3(Δα8) can directly handoff TAs to the chase molecule (upper pathway). Spontaneous TA dissociation from Get3 and binding by the chase (lower pathway) was included in the model for completion.

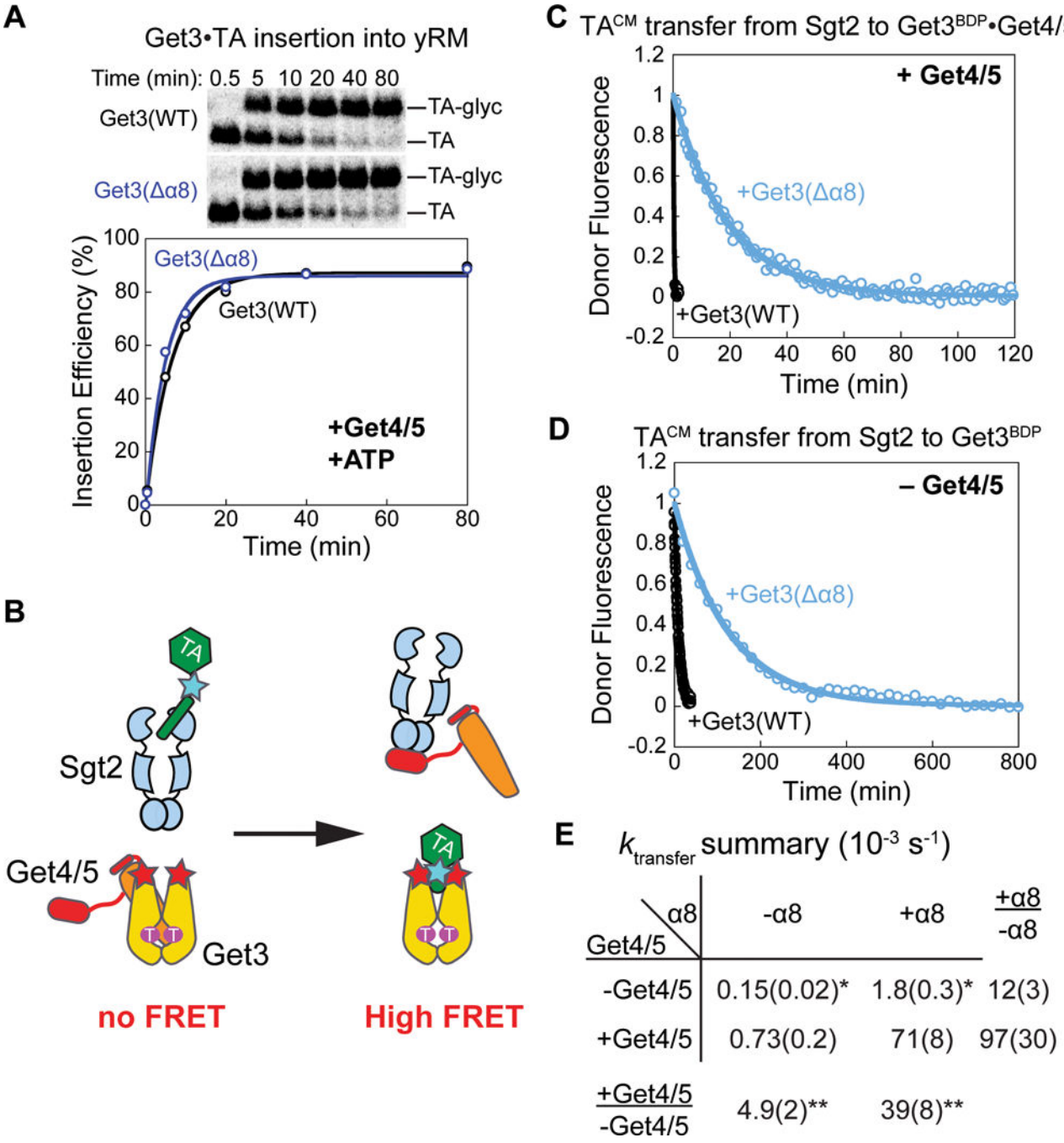

Get4/5 \ α8	-α8	+α8	+α8/-α8
-Get4/5	0.15(0.02)*	1.8(0.3)*	12(3)
+Get4/5	0.73(0.2)	71(8)	97(30)
+Get4/5 / -Get4/5	4.9(2)**	39(8)**	

Figure 2.

α8 and Get4/5 synergistically enable rapid TA transfer from Sgt2 to Get3.

(A) Targeting and translocation of Get3•TA and Get3(Δα8)•TA complexes, performed as described in STAR Methods.

(B) Schematic of the FRET assay to measure TA transfer from Sgt2 to Get3. The cyan and red stars denote the donor and acceptor fluorophores on TA and Get3, respectively.

(C), (D) Donor fluorescence time courses of TA transfer from Sgt2 (25 nM initial Sgt2•TA complex) to 0.3 μM Get3 or Get3(Δα8) with 75 nM Get4/5 present (C), and to 3 μM Get3 or

Get3(Δα8) without Get4/5 present (D). Fluorescence was normalized such that the fit of each trace starts at 1 and ends at 0.

(E) Summary of observed TA transfer rate constants from the data in (C) and (D). Values are reported as mean (SD), with n = 2. Note that the Get4/5-independent TA transfer was measured at a 10-fold higher Get3 concentration than the Get4/5-dependent transfer (indicated by '*'), such that the reported ratios are lower limits for the stimulatory effect of Get4/5 (indicated by '**').

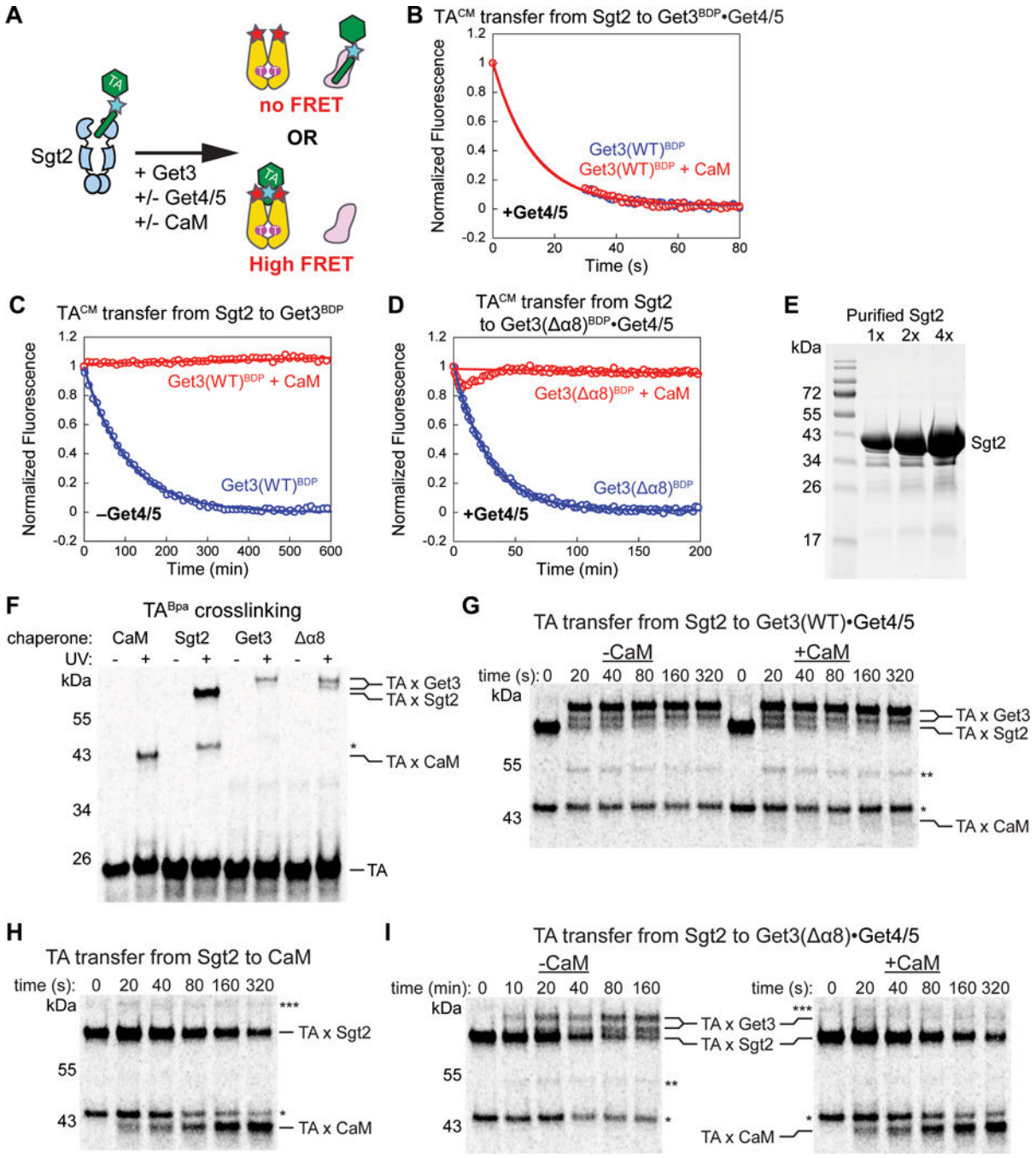

Figure 3.

Both α8 and Get4/5 are required for privileged TA transfer to Get3 in the GET pathway. (A) Schematic of the Sgt2-to-Get3 TA transfer assay in the presence of excess CaM. (B)-(D) In the fluorescence-based transfer assay, CaM did not affect TA transfer from Sgt2 to wild-type Get3•Get4/5 (B), but abolished the changes in donor fluorescence during Get4/5-independent TA transfer from Sgt2 (C) or during transfer from Sgt2 to Get3(Δα8)•Get4/5 (D). Where indicated, reactions contained 25 nM Sgt2•TA, 0.3 μM Get3 or Get3(Δα8), 75 nM Get4/5, and 20 μM CaM.

(E) Visualization of the Sgt2 used for the TA transfer experiments by SDS-PAGE and coomassie blue stain.
(F) SDS-PAGE gel showing TA(Bpa) and its crosslink to different chaperones. '*' denotes a minor crosslinked species in the presence of Sgt2 that was not interpreted.
(G)-(I) Representative SDS-PAGE-autoradiography analyses of the time courses of TA(Bpa) transfer from Sgt2 to 20 μM CaM (H), and to 0.75 μM Get3•Get4/5 (G) or 0.75 μM Get3(Δα8)•Get4/5 (I) with or without 20 μM CaM present. '*', '**', and '***' denote minor crosslinked species that were not interpreted.

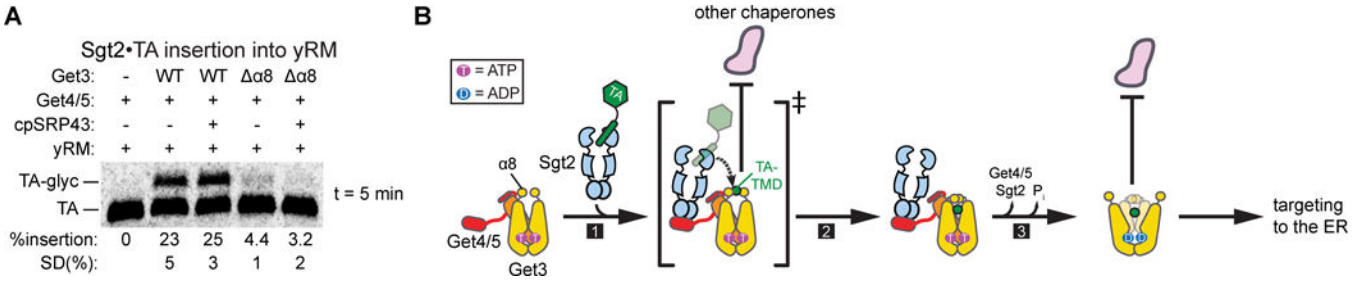

Figure 4.

The α8 lid impacts Get3 function by facilitating TA handover and preventing TA loss to off-pathway chaperones.

(A) TA targeting and insertion assays starting with a preformed Sgt2•TA complex. Values indicate the quantified insertion efficiencies from the representative gel and replicates and are reported as mean ± SD, with n = 3.

(B) Model for the dual roles of α8 as a substrate conduit and a chaperone lid in the GET pathway. Upon interaction of Sgt2•TA with ATP- and Get4/5-bound Get3 (step 1), Get4/5 and the α8 element on Get3 cooperate to enable the formation of a transient transfer intermediate that provides a protected path for TA handover from Sgt2 to Get3. α8 mediates initial contacts with the TA and guides it into the substrate-binding groove on Get3, while also preventing external chaperones from accessing the substrate during the transfer (species in bracket). Get4/5 increases the local concentrations of Sgt2 and Get3 to enable the action of the α8 element. TA loading then induces conformational changes in Get3 that drive its dissociation from Get4/5 and stimulate ATP hydrolysis (step 3). Once the Get3•TA complex is formed and en route to the ER, α8 also acts as a lid to prevent substrate loss to off-pathway chaperones.

KEY RESOURCES TABLE

REAGENT or RESOURCE	SOURCE	IDENTIFIER
Antibodies		
Rabbit polyclonal anti-Kar2p	Peter Walter Lab (UCSF)	N/A
Mouse monoclonal anti-FLAG	GenScript	Cat#A00187; RRID: AB_1720813
Mouse monoclonal anti-PGK1	Abcam	Cat#ab197960
IRDye® 800CW Goat polyclonal anti-Rabbit IgG (H + L)	LI-COR Biosciences	Cat#925–32211; RRID: AB_2651127
IRDye® 800CW Goat polyclonal anti-Mouse IgG (H + L)	LI-COR Biosciences	Cat#925–32210; RRID: AB_2687825
Bacterial and Virus Strains		
E. coli: DH5α	Invitrogen; Thermo Fisher Scientific	Cat#18258012
E. coli: BL21 Star (DE3)	Invitrogen; Thermo Fisher Scientific	Cat#C601003
E. coli: KC6(*ΔslyD*) with pEVOL $tRNA_{CUA}^{opt}$/aaRS	Shu-ou Shan Lab (Caltech)	Saraogi et al., 2011
Chemicals, Peptides, and Recombinant Proteins		
His_6-Get3	U. Chio; Shu-ou Shan Lab (Caltech)	Suloway et al., 2009
His_6-Get3(Δα8)	U. Chio; Shu-ou Shan Lab (Caltech)	Chio et al., 2017b
Get3 ybbR	U. Chio; Shu-ou Shan Lab (Caltech)	Rao et al., 2016
Get3(Δα8) ybbR	U. Chio; Shu-ou Shan Lab (Caltech)	Chio et al., 2017b
His_6-Sgt2	H. Cho; Shu-ou Shan Lab (Caltech)	Rao et al., 2016
Get4/5	U. Chio; Shu-ou Shan Lab (Caltech)	Chartron et al., 2010
Get4(C177T/S48C)/5	U. Chio; Shu-ou Shan Lab (Caltech)	Rome et al., 2014
His_6-Get1CD	U. Chio; Shu-ou Shan Lab (Caltech)	Rome et al., 2014
Intein-cpSRP43	U. Chio; Shu-ou Shan Lab (Caltech)	Liang et al., 2016
Calmodulin-His_6	U. Chio; Shu-ou Shan Lab (Caltech)	Shao and Hegde, 2011
Sfp-His_6	U. Chio; Shu-ou Shan Lab (Caltech)	Yin et al., 2006
His_6-T7 RNA polymerase	U. Chio; Shu-ou Shan Lab (Caltech)	Saraogi et al., 2011
Tagless T7 RNA polymerase	M. Rao; Shu-ou Shan Lab (Caltech)	Rao et al., 2016
Δget3 yeast lysate	M. Rao; Shu-ou Shan Lab (Caltech)	Rome et al., 2013
E. coli S30 lysate	S. Wang; Shu-ou Shan Lab (Caltech)	Saraogi et al., 2011
Δget3 yeast rough microsomes	U. Chio; Shu-ou Shan Lab (Caltech)	Rome et al., 2013
Ni-NTA agarose	Qiagen	Cat#30230
Strep-Tactin Sepharose	IBA Life Sciences	Cat#2–1201-010
Pierce™ anti-HA magnetic beads	Thermo Fisher Scientific	Cat#88836
ATP	Millipore-Sigma	Cat#A2383
ADP	Millipore-Sigma	Cat#A2754
AMPPNP	Jena Bioscience	Cat#NU-407
Calcium acetate hydrate	Millipore-Sigma	Cat#C1000

REAGENT or RESOURCE	SOURCE	IDENTIFIER
PfuTurbo AD with 10X cloned *Pfu* reaction buffer AD	Agilent Technologies	Cat#600255
Deoxynucleotide (dNTP) solution mix	New England BioLabs	Cat#N0447L
L-[^{35}S]-Methionine	Perkin Elmer	Cat#NEG009A005MC
[γ–^{32}P]-ATP	Perkin Elmer	Cat#BLU002A250UC
p-Benzoylphenylalanine (H-p-Bz-Phe-OH)	Bachem	Cat#4017646
7-hydroxycoumaryl ethylglycine	Millipore-Sigma	Cat#792551
Coenzyme A trilithium salt	Millipore-Sigma	Cat#C3019
BODIPY-FL maleimide	Thermo Fisher Scientific	Cat#B10250
Cy3B maleimide	GE Healthcare	Cat#PA63131
ATTO 647N maleimide	ATTO-TEC	Cat#AD647N-45
Critical Commercial Assays		
EasyTag™ EXPRESS^{35}S Protein Labeling Mix	Perkin Elmer	Cat#NEG772002MC
QIAprep Spin Miniprep Kit	Qiagen	Cat#27106
QIAGEN Plasmid Maxi Kit	Qiagen	Cat#12163
QIAquick PCR Purification Kit	Qiagen	Cat#28106
Experimental Models: Organisms/Strains		
S. cerevisiae: *GET3-FLAG* Strain Background: BY4741	This paper	N/A
S. cerevisiae: *GET3*(*Δα8*)-*FLAG* Strain Background: BY4741	This paper	N/A
S. cerevisiae: *Δget3* (*YDL100c::kanMX4*) Strain Background: BY4741	Yeast Knockout Collection (SGDP)	Cat#YSC6273–201935595; Clone ID: 3797
Oligonucleotides		
Primers used are listed in Table S1	N/A	N/A
Recombinant DNA		
Plasmid: pCAS Get3 T173	This paper	Shan Lab Cat#: pSOS3593
Plasmid: pCAS Get3 T342	This paper	Shan Lab Cat#: pSOS3594
Plasmid: pET33b His$_6$-Get3	C. Suloway; Bil Clemons Lab (Caltech)	Suloway et al., 2009; Shan Lab Cat#: pSOS1289
Plasmid: pET33b His$_6$-Get3(Δα8)	U. Chio; Shu-ou Shan Lab (Caltech)	Chio et al., 2017b; Shan Lab Cat#: pSOS3365
Plasmid: pET28a His$_6$-SUMO-Get3 ybbR	U. Chio; Shu-ou Shan Lab (Caltech)	Rao et al., 2016; Shan Lab Cat#: pSOS2252
Plasmid: pET28a His$_6$-SUMO-Get3(Δα8) ybbR	U. Chio; Shu-ou Shan Lab (Caltech)	Chio et al., 2017b; Shan Lab Cat#: pSOS3051
Plasmid: pET33b His$_6$-Sgt2	J. Chartron; Bil Clemons Lab (Caltech)	Rao et al., 2016; Shan Lab Cat#: pSOS1723
Plasmid: pET33b Get4-His$_6$/Get5	J. Chartron; Bil Clemons Lab (Caltech)	Chartron et al., 2010; Shan Lab Cat#: pSOS1401
Plasmid: pET33b Get4(C177T/S48C)-His$_6$/Get5	M. Rome; Shu-ou Shan Lab (Caltech)	Rome et al., 2014; Shan Lab Cat#: pSOS1706
Plasmid: pET33b His$_6$-Get1CD	H. Gristick; Bil Clemons Lab (Caltech)	Rome et al., 2014; Shan Lab Cat#: pSOS1439
Plasmid: pQE His$_6$-cpSRP43(intein)	F. Liang; Shu-ou Shan Lab (Caltech)	Liang et al., 2016; Shan Lab Cat#: pSOS1975

REAGENT or RESOURCE	SOURCE	IDENTIFIER
Plasmid: pRSET-A Calmodulin-His_6	Manu Hegde Lab (MRC LMB)	Shao and Hegde, 2011; Shan Lab Cat#: pSOS3361
Plasmid: pET29 Sfp-His_6	Jun Yin Lab (Georgia State University)	Yin et al., 2006; Shan Lab Cat#: pSOS2068
Plasmid: pK7 3xStrep-SUMOnc-Bos1-opsin	M. Rao; Shu-ou Shan Lab (Caltech)	Rao et al., 2016; Shan Lab Cat#: pSOS2101
Plasmid: pK7 3xStrep-SUMOnc-amberBos1-opsin	M. Rao; Shu-ou Shan Lab (Caltech)	Rao et al., 2016; Shan Lab Cat#: pSOS2353
Plasmid: pK7 3xStrep-SUMOnc-Bos1(A228TAG)-opsin	This paper	Shan Lab Cat#: pSOS3410
Plasmid: pRS316 GPD 3HA-BirA-Bos1-opsin	H. Cho; Shu-ou Shan Lab (Caltech)	Cho and Shan, 2018; Shan Lab Cat#: pSOS2910
Software and Algorithms		
ImageQuant TL	GE Healthcare	RRID: SCR_014246; https://www.gelifesciences.com/en/es/shop/protein-analysis/molecular-imaging-for-proteins/imaging-software/imagequant-tl-8-2-image-analysis-software-p-09518
Image Studio Lite	LI-COR	RRID: SCR_013715; https://www.licor.com/bio/products/software/image_studio_lite/
Kaleidagraph	Synergy	RRID: SCR_014980; http://www.synergy.com/pixelperfect/pixelperfect/kg.htm
Berkeley Madonna	Macey & Oster, UC Berkeley	https://berkeley-madonna.myshopify.com/
FRETBursts	Ingargiola et al.; Shimon Weiss Lab (UCLA)	Ingargiola et al., 2016; https://github.com/OpenSMFS/FRETBursts